Transport properties of optically thin solid dielectrics from frequency correlations of randomly scattered light

Geoffroy J. Aubry, Nathan Fuchs, Sergey E. Skipetrov, Frank Scheffold

Optics Letters

Transport properties of optically thin solid dielectrics from frequency correlations of randomly scattered light

Geoffroy J. Aubry,[1,2,4] Nathan Fuchs,[1] Sergey Skipetrov,[3] and Frank Scheffold[1,5]

[1]Department of Physics, University of Fribourg, 1700 Fribourg, Switzerland
[2]Université Côte d'Azur, CNRS, Institut de Physique de Nice, 06100 Nice, France
[3]Université Grenoble Alpes, CNRS, LPMMC, 38000 Grenoble, France
[4]e-mail: geoffroy.aubry@cnrs.fr
[5]e-mail: frank.scheffold@unifr.ch

Received 29 November 2021; revised 19 January 2022; accepted 29 January 2022; posted 31 January 2022; published 10 March 2022

Frequency-dependent intensity correlation function measurements can be employed to determine the optical turbidity of solid disordered dielectrics. Here we demonstrate a speckle frequency correlation experiment with a focused beam and using an area detector. We show how to apply frequency correlation measurements to optically thin solid samples with the aim of determining the light diffusion coefficient and transport mean free path ℓ^*. To give a practical example, we extract the optical transport mean free path of PTFE (Teflon) slabs, with a thickness of $L = 0.4$–3.5 mm, covering optical densities $L/\ell^* \sim 4$–15.

https://doi.org/10.1364/OL.449084

Nonabsorbing disordered dielectrics, such as films of white paint or optical diffusers, display random wave scattering which leads to Lambertian reflectance and diffuse transmission of light for optically thick samples. The optical thickness of a material is defined by L/ℓ^*, where L denotes the thickness and ℓ^* is the transport mean free path. Typically, for $L \gtrsim 2\ell^*$ wave scattering is random, meaning that we can apply the central limit theorem to describe the scattered wave phase and field amplitude statistical properties [1]. In a more restrictive limit, typically for $L \gtrsim 10\ell^*$, wave scattering and transport are fully diffusive. The terms "light diffusion" and "random wave scattering" are often used interchangeably, but it is essential to notice the difference.

For a coherent light source, the randomly scattered light waves interfere and form a fully developed intensity speckle pattern [1–5]. Upon changing the position of the scatterers, or the wave's frequency, the speckles fluctuate. Transmission diffusing wave spectroscopy (DWS) is a popular method that exploits temporal fluctuations of the speckle intensity to characterize the dynamics inside a turbid sample [2,3]. DWS can also be used to determine the optical thickness L/ℓ^* if the sample's dynamic properties are known. For random scattering, the Siegert relation connects the intensity correlation function, $G_2(\gamma)$, to the field–field correlation function $g_1(\gamma) = \langle E(\gamma)E(0)^*\rangle / \langle |E(0)|^2\rangle$:

$$\frac{G_2(\gamma)}{G_2(0)} = g_2(\gamma) = \frac{\langle I(0)I(\gamma)\rangle}{\langle I(0)\rangle^2} = 1 + |g_1(\gamma)|^2, \tag{1}$$

where $\langle \cdots \rangle$ denotes either an average over many speckles, corresponding to an ensemble average, or, if the sample is liquid and ergodic, an average over time. Depending on the type of correlation studied, we use the γ parameter defined as follows:

$$\begin{cases} \gamma = 0, & \text{for the average intensity} \\ \gamma^2 = \dfrac{k^2}{\ell^{*2}}\langle \Delta r^2(\tau)\rangle, & \text{for the temporal correlation in DWS} \\ \gamma^2 = \dfrac{-i\Delta\omega}{D}, & \text{for the frequency correlation.} \end{cases} \tag{2}$$

Here $\langle \Delta r^2(\tau)\rangle$ is the mean squared displacement of the Brownian particles over a time τ in the case of temporal correlations, $\Delta\omega = 2\pi\Delta\nu$ is the angular frequency difference of the light, and D the light diffusion constant in the case of frequency correlations. Mathematical equivalence between temporal and frequency correlation functions is demonstrated in Supplement 1 (Section 2).

Speckle frequency correlations have been studied since 1990 using tunable laser sources [4,6,7]. More recently, Muskens and Lagendijk proposed broadband spectroscopy through opaque scattering media as a tool for the characterization of random scattering media [8]. Their work is based on simplified diffusion approximation results first published by Genack and co-workers [9,10] in the early 1990s and valid only for optically thick samples, typically $L \gtrsim 10\ell^*$. Here we show how broadband spectroscopy can be implemented also for optically thin samples, $L \gtrsim 4\ell^*$. To study the range of validity of different levels of approximations, we compare the theory used by Muskens and others [4,9,10] with full predictions of the diffusion equation. We note that we have also investigated other models, such as the low-order scattering model of Ref. [11], but could not find further improvement. The expression for the normalized intensity

correlation function $g_2^{\omega}(\Delta\omega)$ commonly used is

$$g_2^{\omega}(\Delta\omega) = 1 + \frac{2\Delta\omega/\omega_0}{\cosh\sqrt{2\frac{\Delta\omega}{\omega_0}} - \cos\sqrt{2\frac{\Delta\omega}{\omega_0}}}, \tag{3}$$

where $D = c_0\ell^*/3n_{\text{eff}}$ is the light diffusion constant with the vacuum speed of light c_0 and a medium effective refractive index n_{eff}. The dimensionless extrapolation length in diffusion theory is set by $\zeta_e \equiv \frac{z_e}{\ell^*} = \frac{2(1+R)}{3(1-R)}$, where $R(n_{\text{eff}})$ denotes the angle-averaged internal reflection coefficient at the sample's interface [12,13] see Eq. (S5) in Supplement 1 or Refs. [12,14]. The characteristic decay frequency is $\omega_0 = D/(L+2z_e)^2$ [4,9,10]. Using (3) together with (1) we can fit experimental data for $g_2^{\omega}(\Delta\omega)$ with ω_0 as an adjustable parameter. For $L \gg \ell^*$ we neglect $z_e \ll L$ and find $\omega_0 \simeq D/L^2$ and thus $\ell^* = \frac{3n_{\text{eff}}L^2\omega_0}{c_0}$. For smaller L/ℓ^*, we need to solve the following equation to determine ℓ^* from ω_0:

$$\underbrace{\frac{4\zeta_e^{\,2}}{L^2}}_{A}\ell^{*2} + \underbrace{\left[\frac{4\zeta_e}{L} - \frac{c_0}{3n_{\text{eff}}\omega_0 L^2}\right]}_{B}\ell^* + 1 = 0. \tag{4}$$

This equation has a real solution only if $B^2 - 4A \geq 0$. If $\omega_0 > \frac{c_0}{24\zeta_e n_{\text{eff}}L}$, $B^2 - 4A < 0$: no real solution can be extracted for ℓ^*. If $\omega_0 = \frac{c_0}{24\zeta_e n_{\text{eff}}L}$, then the smallest possible solution for the optical thickness is reached for $L/\ell^* = 2\zeta_e$ and Eq. (4) thus sets an upper bound.

To understand the limitations imposed by the commonly used model, we consider the diffusion equation, appearing in the analysis of multiple wave scattering in disordered media [15,16]:

$$\left[\frac{\partial^2}{\partial z^2} - \gamma^2\right] C(z,z',\gamma) = -\frac{1}{D}\delta(z-z'). \tag{5}$$

The result for the average intensity, temporal, or frequency correlation functions in transmission of a plane wave through a slab is obtained by setting $z' = \ell^*$ and computing the flux through the plane $z = L$. Details of these routine calculations are included in Supplement 1 (Section 3). We find

$$\begin{aligned} G_1(\gamma) &= -D\,\frac{\partial}{\partial z}C(z,\ell^*,\gamma)\bigg|_{z=L} \\ &= \frac{\gamma z_e^{(0)}\cosh(\gamma\ell^*) + \sinh(\gamma\ell^*)}{\sinh(\gamma L)\left[\gamma^2 z_e^{(0)}z_e^{(L)} + 1\right] + \gamma\left[z_e^{(0)} + z_e^{(L)}\right]\cosh(\gamma L)}, \end{aligned} \tag{6}$$

where we allow for the possibility of having different extrapolation lengths $z_e^{(0)}$ and $z_e^{(L)}$ at the opposite faces $z = 0$ and $z = L$ of the slab. The normalized correlation functions $g_1(\gamma) = G_1(\gamma)/G_1(0)$ are obtained from Eq. (6) by dividing it by the average intensity transmission coefficient $T = G_1(0) = (z_e^{(0)} + \ell^*)/(L + z_e^{(0)} + z_e^{(L)})$. We can recover the previous Eq. (3) by setting $z_e^{(0)} = z_e^{(L)} = 0$ and expanding the result in the limit $L \gg \ell^*$ for details, see Supplement 1 (Section 4) and Ref. [17].

To illustrate the difference between Eqs. (6) and (3), we measure the frequency intensity correlation function of light transmitted through stacks of thin 0.1 mm sheets made of PTFE (Teflon) with a mean free path of $\ell^* \sim 200$ μm at $\lambda \sim 800$ nm, reported in the literature [18]. Depending on the number of sheets used, we vary the slab thickness from $L = 0.4$ mm to $L = 3.5$ mm. We use a single frequency-tunable laser light source (Toptica Photonics, model DL 100 DFB) with a central wavelength of $\lambda \simeq 784.5$ nm. The laser radiation emitted is fed into an optical fiber, collimated by a lens coupled at its end face, and directed onto the front face of the scattering medium. We position the sample in the focal plane of a Nikon Plan Apochromat 20X 0.75 objective, and we guide the scattered light on a digital charge-coupled device (CCD) camera (Ximea xiD MD028MU-SY) where a speckle pattern is formed (see Fig. 1 for the setup). The size of a speckle on the detector is of the order of ~ 20 pixel edge lengths and we probe ~ 1000 independent speckles in our experiment [19]. While sweeping the laser frequency over a maximum frequency range $\Delta\omega_{\text{max}} \in 2\pi \cdot [10, 250]$ GHz (for the thickest/thinnest samples), we record the speckle images and subsequently compute the multi-speckle $g_2^{\omega}(\Delta\omega)$ using standard procedures [18]. We note that $\Delta\omega_{\text{max}} = 250$ GHz corresponds to $\Delta\lambda = 0.5$ nm and we assume that the optical properties remain unchanged over the range of frequencies probed. Compared with the method of Muskens and Lagendijk [8], our camera-based approach provides a better signal-to-noise performance and therefore removes the need to move the sample to average over different speckle realizations.

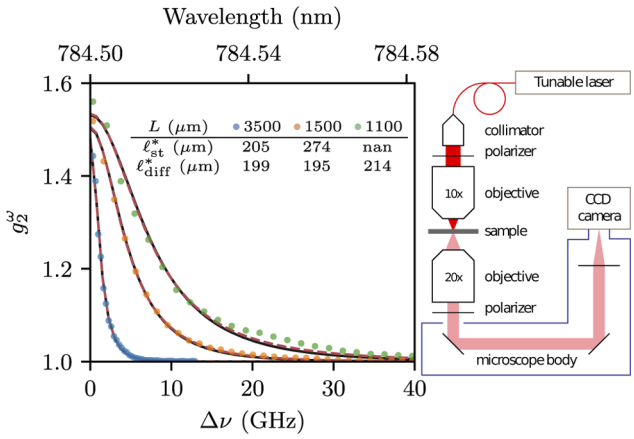

Fig. 1. Left: Typical speckle correlation measurements through stacks of 11, 15, and 35 sheets of PTFE (Teflon) of thickness 100 μm, effective refractive index $n_e = 1.356$. Solid lines are fits with (3) (st) and dashed lines with (6) (diff). The extracted ℓ^* are reported in the table. Right: Experimental setup using a frequency-tunable laser at $\lambda \simeq 784.5$ nm, two microscope objectives, and an area detector (CCD digital camera).

In Fig. 1, we present our experimental results for three different samples of thicknesses 3500, 1500, and 1100 μm (symbols). For each $\Delta\omega$, we record a sequence of four pictures with the following $\Delta\omega$: (1) 0, (2) $\Delta\omega$, (3) 0, (4) $\Delta\omega$, and therefore each point in Fig. 1 is averaged over the three correlations between (1) $\leftrightarrow$ (2), (2) $\leftrightarrow$ (3), and (3) $\leftrightarrow$ (4). For each measurement, the black solid line shows the best fit using Eq. (3), and the red dashed line the fit using Eq. (6). The values of ℓ^* extracted by both methods are shown in the table in Fig. 1. For the thickest sample (3500 μm), both methods give similar ℓ^*. This is not the case for the two other samples: for $L = 1500$ μm, the values are different, and for $L = 1100$ μm, it is no longer possible to extract a real ℓ^* value by solving Eq. (4). These different results are not related to the fit quality, since the fitted curves are almost indistinguishable in Fig. 1.

In order to quantify the validity range of both methods, we measured different samples of thicknesses between 0.4 and 3.5 mm. The extracted ℓ^* are plotted as symbols in Fig. 2. For optically thick samples, $L/\ell^* \simeq 10$, we find good agreement between

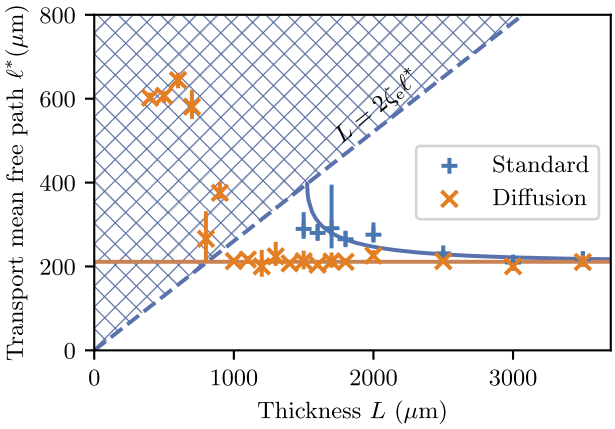

Fig. 2. Symbols: transport mean free paths measured on Teflon stacks of different thicknesses L. Blue +: $\ell^*_{\rm st}$ obtained using the standard formula [Eqs. (3) and (4)]. Orange ×: $\ell^*_{\rm diff}$ obtained using the full expression Eq. (6). Solid orange curve (bottom): $\ell^*_{\rm diff,av}$, average taken over full diffusion theory data (orange symbols) for $L \geq 1500$ μm. Solid blue curve (top): $\ell^*_{\rm st}$ calculated from Eq. (4) with $D = c_0\ell^*_{\rm diff,av}/3n_{\rm eff}$. Dashed line: for $L<2\zeta_e\ell^*$, Eq. (4) has no solutions (area indicated by the cross-hatching).

the results obtained using the approximate model (3) by Genack *et al.* and our more accurate expression (6) derived from full diffusion theory. However, for $L/\ell^*<7$ ($L<1500$ μm) the approximation (3) fails to provide any meaningful prediction for ℓ^*, while the full expression makes accurate predictions down to $L/\ell^* = 4$. Our findings are in agreement with a DWS study by Kaplan *et al.* [20] based on diffusion theory modeling, Eq. (6) for DWS applied to measurements on samples with a scattering anisotropy g close to one. For comparison, $g_{\rm Teflon} \sim 0.9$ [18]. Note that Kaplan *et al.* studied also more isotropic scatterers with $g \sim 0$. In the latter case DWS experiments suggest deviations between experiment and theory already for $L/\ell^* \leq 5$–7 [20]. Since static samples with $g \sim 0$ are not readily available, we have not performed frequency correlation experiments in this regime.

To quantify the differences between Eqs. (3), (4), and our Eq. (6), we set $\ell^*_{\rm diff,av} = 211$ μm [the average of ℓ^* extracted using Eq. (6) for $L \geq 1500$ μm] and calculate $g_2^\omega(\Delta\omega)$ for different values of L. Using the simple analytical Eq. (3), we fit these curves to obtain $\ell^*_{\rm st}$. In Fig. 2 we plot the results of these fits (blue solid line) for a medium having an effective refractive index (in air) of $n_{\rm eff} = 1.356$ corresponding to $z_e/\ell^* = 1.92$. As expected, for $L/\ell^* \to \infty$ the results obtained from (3) are the same as those following from (6). Clear deviations appear for smaller values of L/ℓ^*. The value of $\ell^*_{\rm st}$ increases when L decreases, and, at some point, reaches the critical value above which Eq. (4) no longer has a real solution in the half plane $L<2\zeta_e\ell^*$. The boundary is plotted as a dashed line in Fig. 2. Revealing the catastrophic failure of the commonly used Eq. (3) is the central result of our work.

In summary, we implemented a speckle frequency correlation experiment using an area detector and have measured $g_2^\omega(\Delta\omega)$ for PTFE (Teflon) slabs of different thicknesses. Based on diffusion theory, we derived a theoretical model of frequency correlation measurement featuring proper accounting for boundary conditions that can be different on opposite sides of the sample. We have shown that such an approach is necessary and accurate since the standard method fails catastrophically for small L/ℓ^*. Our improved modeling demonstrates that speckle correlation experiments can be analyzed quantitatively and could thus become a valuable tool for characterizing optically thin solid samples down to $L/\ell^* \sim 4$. Since the frequency correlation experiments can be performed with a focused laser beam, in contrast, for example, to coherent backscattering cone measurements [21,22], we can apply our method even to small samples of microscopic lateral size [23].

Funding. National Center of Competence in Research Bio-Inspired Materials (182881); Schweizerischer Nationalfonds zur Förderung der Wissenschaftlichen Forschung (169074, 188494).

Disclosures. The authors declare no conflicts of interest.

Data availability. Data underlying the results presented in this paper are not publicly available at this time but may be obtained from the authors upon reasonable request.

Supplemental document. See Supplement 1 for supporting content.

REFERENCES

1. J. C. Dainty, *Laser Speckle and Related Phenomena* (Springer, 2013).
2. G. Maret and P. E. Wolf, Z. Phys. B: Condens. Matter **65**, 409 (1987).
3. D. J. Pine, D. A. Weitz, P. M. Chaikin, and E. Herbolzheimer, Phys. Rev. Lett. **60**, 1134 (1988).
4. M. P. van Albada, J. F. de Boer, and A. Lagendijk, Phys. Rev. Lett. **64**, 2787 (1990).
5. C. W. Hsu, S. F. Liew, A. Goetschy, H. Cao, and A. D. Stone, Nat. Phys. **13**, 497 (2017).
6. A. A. Duran-Ledezma, D. Jacinto-Méndez, and L. F. Rojas-Ochoa, Appl. Opt. **57**, 208 (2018).
7. A. A. Duran-Ledezma, H. A. D. L. Cruz-Burelo, and L. F. Rojas-Ochoa, J. Opt. Soc. Am. A **37**, 1650 (2020).
8. O. L. Muskens and A. Lagendijk, Opt. Lett. **34**, 395 (2009).
9. A. Z. Genack, Phys. Rev. Lett. **58**, 2043 (1987).
10. A. Z. Genack and J. M. Drake, Europhys. Lett. **11**, 331 (1990).
11. P.-A. Lemieux, M. U. Vera, and D. J. Durian, Phys. Rev. E **57**, 4498 (1998).
12. J. X. Zhu, D. J. Pine, and D. A. Weitz, Phys. Rev. A **44**, 3948 (1991).
13. J. Haberko, L. S. Froufe-Pérez, and F. Scheffold, Nat. Commun. **11**, 4867 (2020).
14. M. Vera and D. J. Durian, Phys. Rev. E **53**, 3215 (1996).
15. F. Scheffold, S. E. Skipetrov, S. Romer, and P. Schurtenberger, Phys. Rev. E **63**, 061404 (2001).
16. E. Akkermans and G. Montambaux, *Mesoscopic Physics of Electrons and Photons* (Cambridge University Press, 2011).
17. J. F. de Boer, M. P. van Albada, and A. Lagendijk, Phys. Rev. B **45**, 658 (1992).
18. L. F. Rojas, M. Bina, G. Cerchiari, M. A. Escobedo-Sánchez, F. Ferri, and F. Scheffold, Eur. Phys. J. Spec. Top. **199**, 167 (2011).
19. S. E. Skipetrov, J. Peuser, R. Cerbino, P. Zakharov, B. Weber, and F. Scheffold, Opt. Express **18**, 14519 (2010).
20. P. Kaplan, M. H. Kao, A. Yodh, and D. J. Pine, Appl. Opt. **32**, 3828 (1993).
21. M. Chen, D. Fischli, L. Schertel, G. J. Aubry, B. Häusele, S. Polarz, G. Maret, and H. Cölfen, Small **13**, 1701392 (2017).
22. G. J. Aubry, L. Schertel, M. Chen, H. Weyer, C. M. Aegerter, S. Polarz, H. Cölfen, and G. Maret, Phys. Rev. A **96**, 043871 (2017).
23. M. Burresi, L. Cortese, L. Pattelli, M. Kolle, P. Vukusic, D. S. Wiersma, U. Steiner, and S. Vignolini, Sci. Rep. **4**, 6075 (2014).